

Towards a better understanding of trench defects in InGaN/GaN quantum wells

F C-P Massabuau, L Trinh-Xuan, D Lodié, S -L Sahonta, S Rhode, E J Thrush, F Oehler, M J Kappers, C J Humphreys and R A Oliver

Department of Materials Science and Metallurgy, University of Cambridge, Pembroke Street, Cambridge CB2 3QZ, United Kingdom

E-mail: fm350@cam.ac.uk

Abstract. Trench defects are a commonly occurring feature in InGaN/GaN quantum well (QW) structures. This defect appears at the surface of a structure as a trench enclosing a region of material with peculiar emission properties. Transmission electron microscopy was used to characterise the sub-surface structure of such defect. It consists of a basal-plane stacking fault (BSF) located in the QW stack and bound by a vertical stacking mismatch boundary (SMB) which runs towards the surface and which opens up into pits, which merge to form a trench. Atomic force microscopy and cathodoluminescence were performed on the same individual defects in order to directly correlate the morphology with the emission properties. A strong correlation has been established between the thickness of the trench and the redshift and intensity of the emission of the enclosed region suggesting that bright trench defects emitting at a longer wavelength nucleate early during the growth. Data also suggest that the SMB may act as a non-radiative recombination centre.

1. Introduction

InGaN/GaN quantum well (QW) structures are a key component of high efficiency opto-electronic devices [1]. However, such structures are characterised by a high density of defects such as threading dislocation [2], V-pits [3] and trench defects (trenches at the surface of the structure enclosing a region of material) [4], which might affect their optical properties. Although threading dislocations and V-pits have attracted an intense research effort, trench defects are still poorly understood.

This study investigates the structure of trench defects by transmission electron microscopy (TEM) and tries to link the morphology of a defect with its optical properties using a “multi-microscopy analysis” based on atomic force microscopy (AFM) and scanning electron microscopy with cathodoluminescence (SEM-CL).

2. Experimental methods

InGaN/GaN multiple QW structures were grown by metal-organic vapour phase epitaxy (MOVPE) in a Thomas Swan 6 x 2-inch close-coupled reactor. Trimethylgallium (TMG), trimethylindium (TMI) and ammonia (NH₃) were used as precursors with H₂ as the carrier gas for GaN growth and with N₂ as the carrier gas for InGaN growth. GaN pseudo-substrates grown on *c*-plane (0001) sapphire with a miscut of $0.25 \pm 0.10^\circ$ towards (11-20) were employed. Following the growth of approximately 2.2 nm of In_{0.175}Ga_{0.825}N at 745°C, a protective capping layer of about 1 nm of GaN is grown at 745°C. Then the



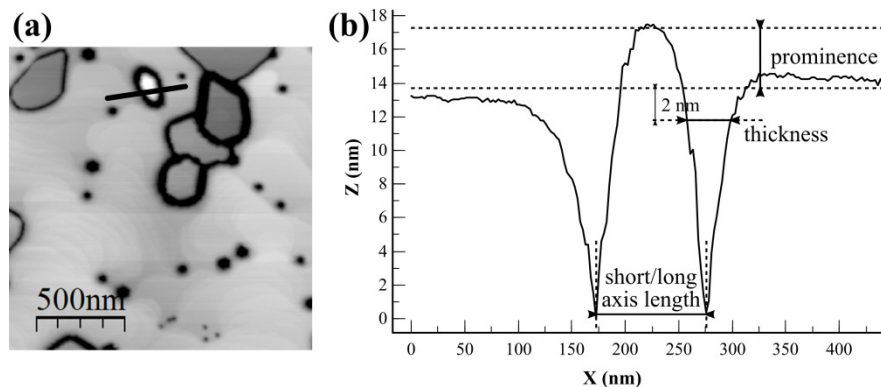


Figure 1. (a) AFM image of trench defects and (b) line profile associated with the black line in (a) illustrating the metrics recorded.

growth of GaN continues while the temperature is ramped-up to 860°C, the growth temperature is maintained at 860°C till 7.5 nm of GaN in total is grown. The thicknesses and composition of the structure were assessed by X-ray diffraction using Vickers *et al.*'s method [5].

AFM in tapping mode was performed to assess the morphology of the defects. Figure 1 shows a typical AFM image of trench defects (figure 1(a)) and illustrates the metrics which are used to characterise the defects' geometry (figure 1(b)): data about the prominence, thickness and area of about 200 defects were collected. The prominence corresponds to the difference in height between the enclosed region of the defect and the average height of the surrounding area. The thickness was measured as the thickness of the V-shaped ditch 2 nm below the level of the surrounding area. Finally, approximating a trench defect as an ellipse, the area was calculated using the measurements for the short and long axis length of the ellipse (measured at the bottom of the ditch on both sides of the defect).

SEM and CL were carried out on the same defects using a process explained elsewhere [6]. Emission spectra were recorded along a line going from the surrounding material on one side of a trench defect to the surrounding material on the other side. Using a two-Gaussian peak model to fit the data as described in reference [6], the redshift and intensity ratio were recorded. The redshift corresponds to the difference between the peak emission wavelength of the material enclosed within the defect and the peak emission wavelength of the surrounding material. According to this definition, a positive value of the redshift means that the inner region of the trench defect emits at a higher wavelength than the surrounding material. Finally, the intensity ratio corresponds to the ratio between the integrated intensity emitted from the enclosed region of a defect and the integrated intensity from the surrounding region. Therefore, according to this definition, an intensity ratio above unity relates to a trench defect with an enclosed region emitting more intense light than its surroundings.

3. Results

3.1. Sub-surface observation

The structure of trench defects was investigated by TEM. It can be seen in figure 2(a) that a basal plane stacking fault (BSF) is located in the QW stack below the defect. The BSF is observed to be bound by a stacking mismatch boundary (SMB) [7] which runs vertically to the apex of the V-shaped ditch (figure 2(d)). In plan view, the SMB is observed to consist of many straight segments oriented at 60° to each other (figure 2(b)). Thickness reduction fringes associated with a V-pit are observed in figure 2(c), therefore considering the facets of a V-pit are towards $\{1-101\}$ [8], it can be inferred that the SMB is oriented parallel to $\langle 1-100 \rangle$. Moreover, hexagonal fringes similar to that of a V-pit are observed around the SMB and their centre matches with the change in orientation of the SMB.

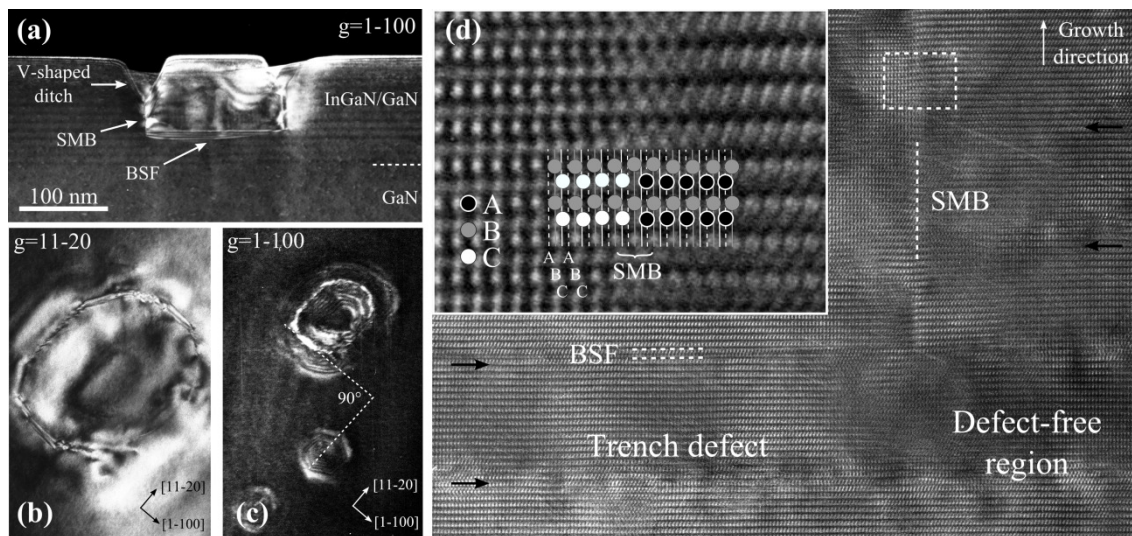


Figure 2. (a) Dark field cross-sectional TEM image of a trench defect using $g = 1-100$. Dark field plan-view TEM image of a same trench defect using $g = 11-20$ (b) and $g = 1-100$ (c). (d) High-resolution TEM image of the SMB. The position of the InGaN QWs is indicated with black arrows. The inset represents a Wiener filtered magnified region of the broken line box.

Hence, trench defects are in fact made of a BSF located in the QW stack and terminated by a SMB. The vertical SMB is oriented parallel to $\langle 1-100 \rangle$ and a hexagonal pit is generated whenever a change of orientation of the SMB occurs, and the coalescence of these pits results in the trench feature which is observed at the sample surface.

3.2. Correlation between morphology and optical properties

A “multi-microscopy analysis” has been performed in order to link the morphology characterised by AFM to the emission properties of exactly the same defects observed by CL (inset of figure 3(a)). It was observed that while the surface area of the enclosed material, measured by AFM, was completely unrelated to the emission, a slight correlation could be established between the prominence of the inner region and the redshift [6]. This trend can be explained by the increased QW thickness which is associated with the growth of additional material in the enclosed region, thus emitting light at a longer wavelength. Finally, a strong correlation has been established between the thickness of the V-shaped ditch and both redshift and intensity ratio (figure 3). Considering the sub-surface structure of the defect, the trench thickness relates to the depth at which the SMB opens up into a pit. Therefore a thick trench necessarily results from an SMB located deep into the QW stack and therefore to a BSF that nucleated at the early stages of the QW growth (configuration 1 in figure 3(a)).

4. Discussion

Although it remains unclear why the enclosed region within a trench defect can emit light at a higher intensity than its surrounding material, figure 3(b) can be exploited to unveil information about the SMB. It has already been described that a wide trench relates to defects with a BSF located at the bottom of the QW stack (configuration 1 in figure 3(b)). But for thin trenches – i.e. defects where the SMB generates pits close to the surface, two extreme cases arise: either the SMB is short and thus the BSF is located close to the surface (configuration 2a in figure 3(b)), or the SMB is long and therefore the BSF is located at the bottom of the stack (configuration 2b in figure 3(b)). By comparing a defect in configuration 1 (for which the intensity is high) and a defect in configuration 2b (for which the intensity is much lower), it can be inferred that the presence of the SMB running through a significant part of the QW stack induces a loss of intensity. Therefore the SMB may act as a non-radiative recombination centre.

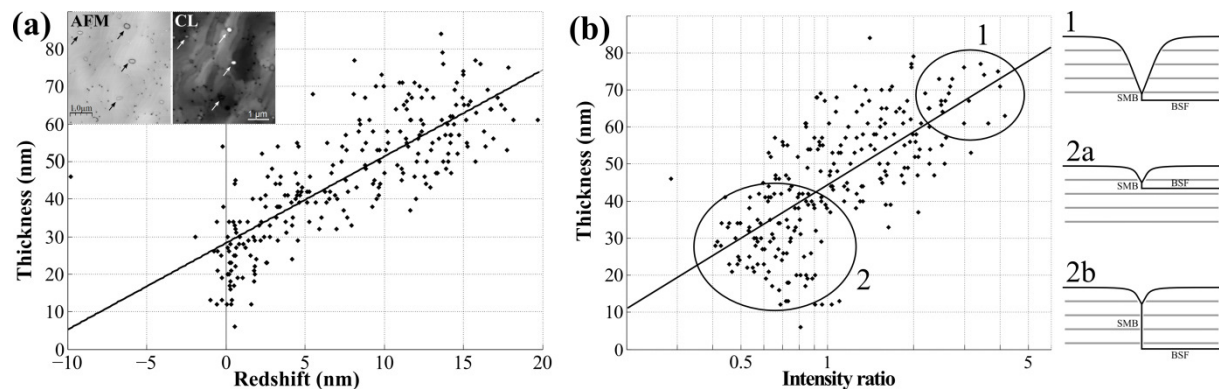


Figure 3. (a) Correlation between the thickness of trench defects and their redshift. The inset illustrates how AFM and CL were performed on the same features. (b) Correlation between the thickness of trench defects and the intensity ratio.

5. Conclusion

The structure of trench defects has been investigated by TEM. It consists of a BSF bound by a vertical $\langle 1-100 \rangle$ -oriented SMB which opens up as hexagonal pits whenever it changes orientation.

A “multi-microscopy analysis” involving AFM and CL has been performed in order to correlate the morphology and emission of these defects. It results that in order to emit a more intense light at a longer wavelength, defects need to have their BSF located deep into the QW stack. It is also suggested that the SMB may act as a non-radiative recombination centre.

References

- [1] Nakamura S, Mukai T, and Senoh M 1994 *Appl. Phys. Lett.* **64** 1687
- [2] Bennett S E 2010 *Materials Science and Technology* **26** 1017
- [3] Wu X H, Elsass C R, Abare A, Mack M, Keller S, Petroff P M, DenBaars S P, Speck J S and Rosner S J 1998 *Appl. Phys. Lett.* **72** 692
- [4] Bruckbauer J, Edwards P R, Wang T, and Martin R W 2011 *Appl. Phys. Lett.* **98** 141908
- [5] Vickers M E, Kappers M J, Smeeton T M, Thrush E J, Barnard J S and Humphreys C J 2003 *J. Appl. Phys.* **94** 1565
- [6] Massabuau F C -P, Trinh-Xuan L, Lodié D, Thrush E J, Zhu D, Oehler F, Zhu T Z, Kappers M J, Humphreys C J and Oliver R A 2013 *J. Appl. Phys.* **113** 073505
- [7] Cho H K, Lee J Y, Kim C S, Yang G M, Sharma N and Humphreys C 2001 *J. Cryst. Growth* **231** 466
- [8] Kim I -H, Park H -S, Park Y -J and Kim T 1998 *Appl. Phys. Lett.* **73** 1634